ELSEVIER

International Journal of Applied Earth Observation and Geoinformation 6 (2005) 261–270

INTERNATIONAL JOURNAL OF APPLIED EARTH OBSERVATION AND GEOINFORMATION

www.elsevier.com/locate/jag

Texture-based landform segmentation of LiDAR imagery

Arko Lucieer*, Alfred Stein

International Institute for Geo-Information Science and Earth Observation (ITC), Department of Earth Observation Science (EOS), P.O. Box 6, 7500 AA Enschede, The Netherlands

Accepted 15 October 2004

Abstract

In this study, we implement and apply a region growing segmentation procedure based on texture to extract spatial landform objects from a light detection and ranging (LiDAR) digital surface model (DSM). The local binary pattern (LBP) operator, modeling texture, is integrated into a region growing segmentation algorithm to identify landform objects. We apply a multi-scale LBP operator to describe texture at different scales. The paper is illustrated with a case study that involves segmentation of coastal landform objects using a LiDAR DSM of a coastal area in the UK. Landform objects can be identified with the combination of a multi-scale texture measure and a region growing segmentation. We show that meaningful coastal landform objects can be extracted with this algorithm. Uncertainty values provide useful information on transition zones or fuzzy boundaries between objects.

Keywords: Multi-scale texture; Region growing; Landform objects; Local binary pattern (LBP) operator

1. Introduction

Object-oriented approaches to remotely sensed image processing have become popular with the growing amount of high-resolution satellite and airborne imagery. Segmentation extracts spatial objects from an image (Gorte and Stein, 1998; Lucieer and Stein, 2002). It extends classification, as spatial contiguity is an explicit goal, whereas it is only implicit in classification. Fisher et al. (2004) show that landform objects have a fuzzy nature. A straightforward approach to identify fuzzy objects is to apply a fuzzy *c*-means (FCM) classification. This classifier gives membership values of belonging to a class. The main shortcoming of pixel-based approaches, such as a standard FCM classifier, is that these methods do not take into account spatial relations between pixel values, also known as pattern or texture. We argue that a texture-based approach applying segmentation (i.e. including the spatial component) can help to identify fuzzy objects.

Cheng and Molenaar (2001) proposed a fuzzy analysis of dynamic coastal landforms, classifying beach, foreshore and dune area as fuzzy objects. Some classification errors, however, may occur as only

* Corresponding author. Tel.: +31 53 4874256.
E-mail address: arko@lucieer.net (A. Lucieer).

0303-2434/$ – see front matter
doi:10.1016/j.jag.2004.10.008

elevation was used as diagnostic information. For example, an area of low elevation behind the foredune is classified as beach, whereas it is almost certainly an area of wind-blown sand removal. Such errors might be reduced by using spatial or contextual information, i.e. by considering morphometry or landforms. Cheng et al. (2002) and Fisher et al. (2004) propose a multi-scale analysis for allocating fuzzy memberships to morphometric classes. This can be used to model objects that are vague for scale reasons. Although this analysis fails to identify positions of dunes, it is possible to identify dune ridges and slacks and to monitor their changing positions.

Regions with a similar reflection can easily be identified as objects on a remote sensing image. In case of a digital surface model (DSM) we can use elevation similarity as a criterion to identify landform objects. These objects, however, are often characterized by more than just elevation. A dune ridge, for example, has a characteristic profile and/or shape, which shows a unique texture in a DSM. Therefore, we argue that texture is an important property of landform objects and should therefore be taken into account in landform analysis. We define texture as a pattern or characteristic spatial variability of pixels over a region. The pattern may be repeated exactly, or as a set of small variations, possibly as a function of position. There is also a random aspect to texture, because size, shape, color and orientation of pattern elements (sometimes called textons) can vary over the region.

Texture measures are used to quantify texture. We split texture measures into structural (transform-based), statistical and combination approaches. Well-known structural approaches are the Fourier and wavelet transform. Several measures can be used to describe these transforms, such as entropy, energy and inertia (Nixon and Aguado, 2002). A well known statistical approach is the grey level co-occurrence matrix (GLCM) (Haralick et al., 1973) containing elements that are counts of the number of pixel pairs for specific brightness levels. Other texture descriptors are Markov random fields (GMRF), Gabor filter, fractals and wavelet models. A comparative study of texture classification is given in Randen and Husøy (1999). They conclude that a direction for future research is the development of powerful texture measures that can be extracted and classified with a low computational complexity. A relatively new and simple texture model is the local binary pattern (LBP) operator (Pietikäinen et al., 2000; Ojala et al., 2002). It is a theoretically simple yet efficient approach to grey scale and rotation invariant texture classification based on local binary patterns.

In this study, we implement and apply a region growing algorithm based on textural information from the LBP operator to extract landform objects from a DSM. To identify these objects we argue that texture is of utmost importance. A description of texture reflects the spatial structure of elevation and slopes, and is therefore indispensable in segmenting an area into sensible landform units. We start by modeling texture using the LBP operator at different scales. Then, we form objects by seeded region growing. We start at the finest pixel level and cluster pixels to form objects, based on textural homogeneity. Growing of objects is stopped if a certain threshold is exceeded. A similarity measure is used to determine whether a pixel can be merged with an object. This measure also provides useful information on extensional uncertainty of objects, expressing uncertainty in their spatial extent. We expect that pixels in transition zones show higher uncertainty values than pixels in core areas with homogeneous textures. To illustrate the use of texture-based segmentation for identification of landform objects, we use a LiDAR DSM of a coastal area in northwest England. This study builds on work of Lucieer and Stein (2002) and Lucieer et al. (2003) and further explores the use of multi-scale texture segmentation to identify landform objects and to quantify their extensional uncertainty.

2. Methods

2.1. Texture model—the local binary pattern (LBP) operator

Ojala et al. (2002) derive the local binary pattern (LBP) operator by defining texture T in a local neighborhood of a grey scale image as the joint distribution of grey levels of P image pixels:

$$T = t(g_c, g_0, \ldots, g_{P-1}) \quad (1)$$

where g_c corresponds to the value of the centre pixel (p_c) of the local neighborhood and g_i ($i = 0, \ldots, P-1$) corresponds to the value of a pixel in the neighborhood of p_c. A circle of radius R with P equally spaced pixels is applied to form a circular symmetric neighborhood set (Fig. 1a).

Invariance with respect to the scaling of pixel values or illumination differences is achieved by

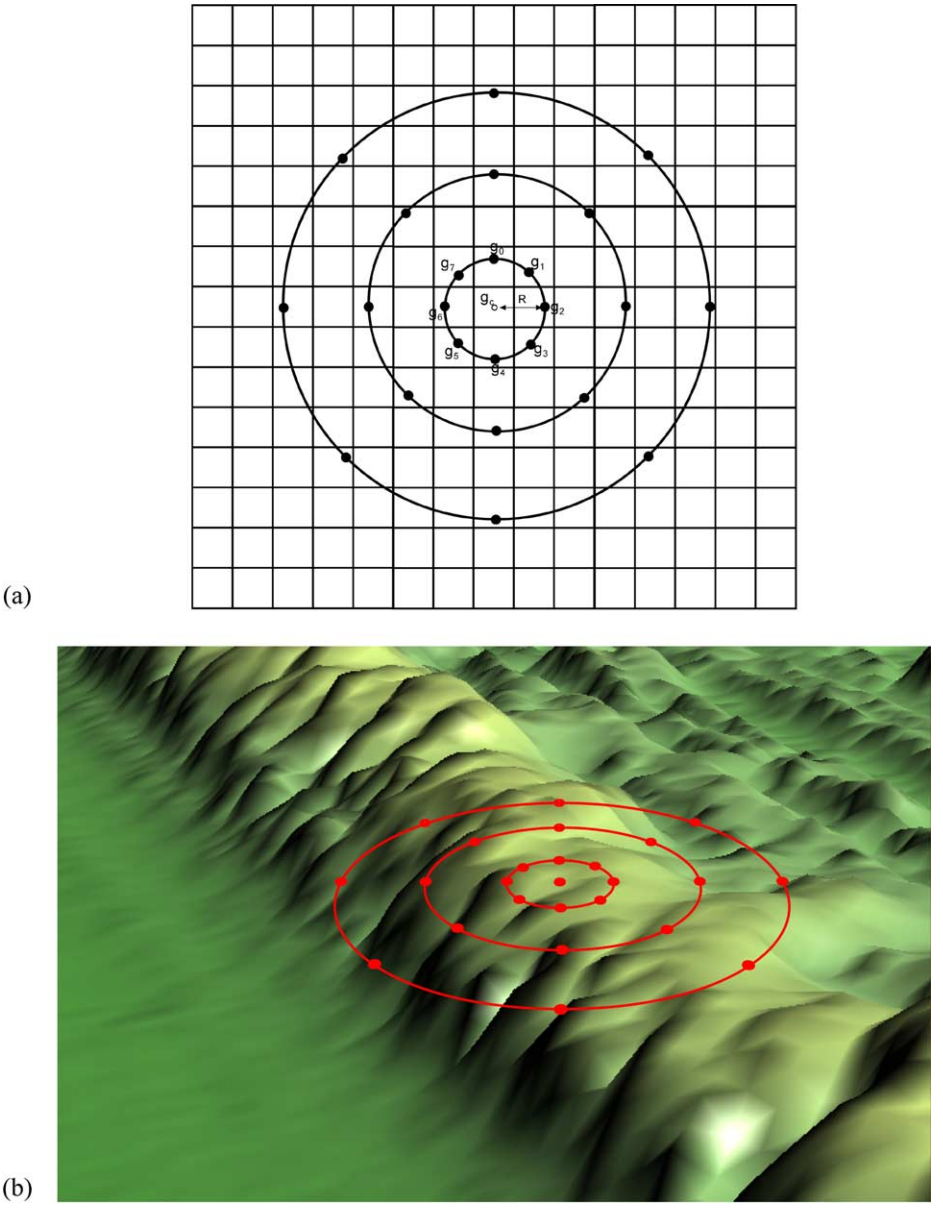

Fig. 1. LiDAR DSM (a) multi-scale circular pixel neighborhood set for different values of P and R; (b) circular neighborhood set draped over a 3D representation of a LiDAR DSM to show its value for describing landforms.

considering the signs of the differences instead of their numerical values:

$$T^* \approx t(\text{sign}(g_0 - g_c), \text{sign}(g_1 - g_c), \ldots, \text{sign}(g_{P-1} - g_c)) \quad (2)$$

This results in the following operator for grey scale and rotation invariant texture description

$$\text{LBP}_c^{P,R} = \sum_{i=0}^{P-1} \text{sign}(g_i - g_c) \quad (3)$$

The $\text{LBP}_c^{P,R}$ operator thresholds pixels in a circular neighborhood of P equally spaced pixels on a circle of radius R, at the value of the centre pixel. It allows for detecting patterns for any quantization of the angular space and for any spatial resolution.

2.2. Multi-scale texture

The $\text{LBP}_c^{P,R}$ measures the spatial structure of local image texture, but discards contrast, being another important property of local image texture. In most cases, its performance can be enhanced by combining it with a rotation invariant variance measure that characterizes the contrast of local image texture, defined by

$$\text{VAR}_c^{P,R} = \sum_{i=0}^{P-1} (g_i - \mu_c)^2, \quad \text{where } \mu_c = \frac{1}{P} \sum_{i=0}^{P-1} g_i \quad (4)$$

To include texture at different scale levels, we take N neighborhood sets at different radii to calculate local binary patterns (Fig. 1a). For each neighborhood set we calculate $\text{LBP}_c^{P,R}$ and $\text{VAR}_c^{P,R}$. We define a multi-scale texture measure LBP_c^N by

$$\text{LBP}_c^N = \sum_{n=1}^{N} \text{LBP}_c^n \quad (5)$$

where n is a combination of P and R. Similarly, the multi-scale variance measure VAR_c^N is calculated over all neighbors at different radii. Fig. 1b illustrates why a multi-scale neighborhood might be seen appropriate for landform description.

2.3. Texture-based image segmentation

To identify and extract landform objects we apply a seeded region growing image segmentation algorithm (Horowitz and Pavlidis, 1976; Haralick and Shapiro, 1985). The initialization of seed pixels is an important issue, because it strongly influences the segmentation result. A random initialization of seeds is a first possibility, however, for every segmentation a different result would be obtained. Alternatively, we start segmentation at locations with minimum local variance. To calculate local variance we apply Eq. (4) with $P = 8$ and $R = 1$, corresponding to a 3×3 kernel, to every pixel in the image. Next, we sort the list of pixels based on variance and start segmentation at pixels with the lowest variance. A similarity criterion is used to merge adjacent pixels to form an image object. For a single band, we use the difference between the mean value of an object and the value of an adjacent pixel. For multiple bands, the angle between the mean vector of an object and the feature vector of an adjacent pixel is used. We select the mean angle difference of all pixels in the image as a threshold to determine whether a pixel can be merged with an object.

After the initial growing phase, no more pixels can be merged with existing objects with similarity values lower than the selected threshold. Then, new seeds are placed to form new objects. This process is continued until all image pixels are merged with an object. In the next phase, adjacent objects are merged according to the same similarity criterion. The difference in object mean values (single band) or the spectral angle between mean vectors of objects (multiple bands) is used to assess whether objects can be merged. Merging is continued until stable image segmentation is obtained.

Information on texture might provide useful information for identification of objects. We extend the standard region growing algorithm by using the multi-scale LBP_c^N and VAR_c^N measures as a basis for segmentation. The purpose is to identify objects based on texture homogeneity. As pixels with a low similarity are merged with an object with higher uncertainty, we use pixel similarity measures to depict extensional uncertainty. The similarity measure is scaled and inversed to obtain a normalized uncertainty value between 0.0 and 1.0. Transition zones between objects can be identified with this uncertainty measure.

3. Case study

3.1. Study area: the Ainsdale Sands

The study area (6 km^2) is on the coast of Northwest England named Ainsdale Sands. The Ainsdale Sand Dunes National Nature Reserve (NNR) totals 508 ha and forms part of the Sefton Coast, on the northwest coast of England. The NNR is within the coastal special protection area. The NNR contains a range of habitats, including intertidal sand flats, embryo dunes, high mobile yellow dunes, fixed vegetated dunes, wet dune slacks, areas of deciduous scrub and a predominantly pine woodland. Management of this area consists of extending the area of open dune habitat through the removal of pine plantation,

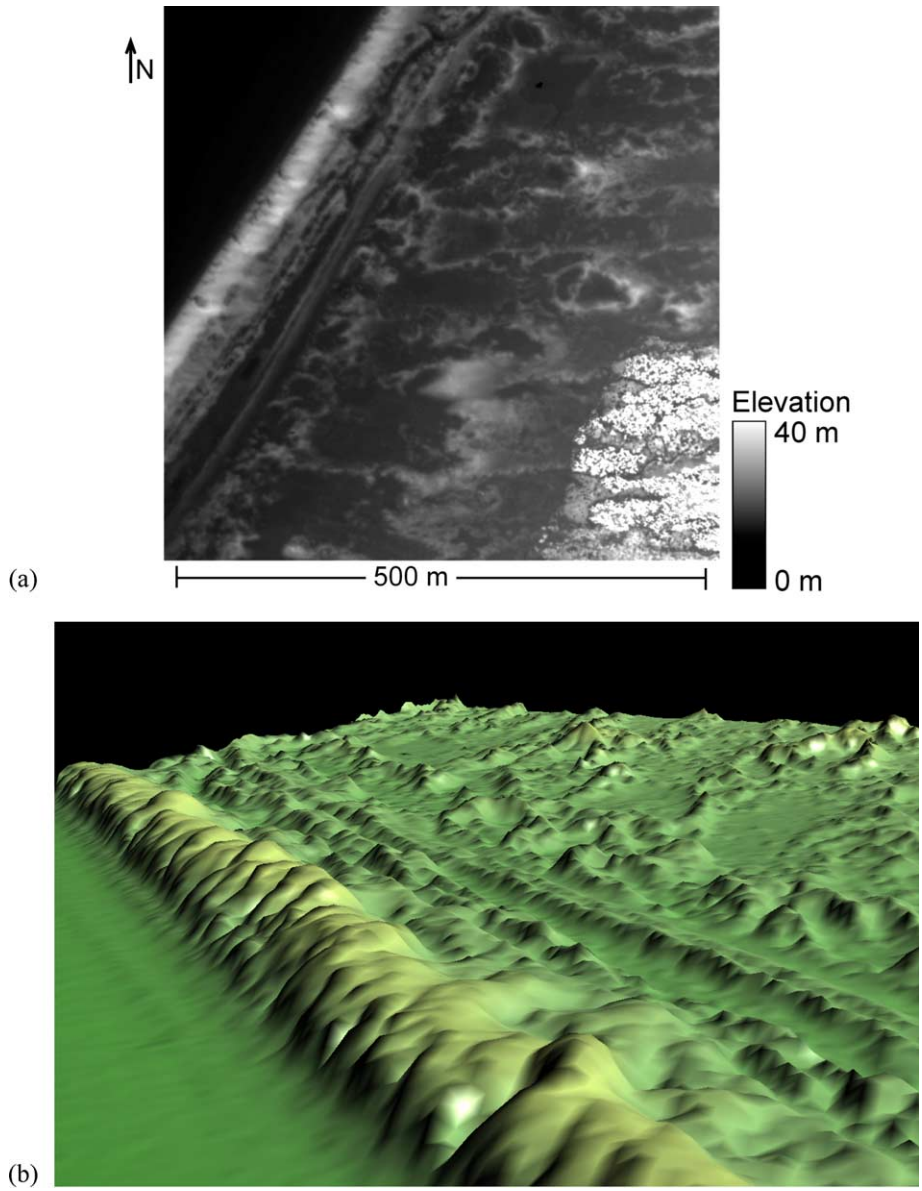

Fig. 2. Digital surface model of the study area: (a) LiDAR DSM; (b) 3D view of foredune and dune field.

maintaining and extending the area of fixed open dune by grazing and progressively creating a more diverse structure within the remaining pine plantation with associated benefits for wildlife (Ainsdale Sand Dunes NNR, 2003). Therefore, mapping of this coastal area is important for protection and management of the environment and as a defense against coastal flooding.

3.2. LiDAR DSM

In 1999–2001 the Environment Agency, UK, collected high-resolution LiDAR imagery, and simultaneously, acquired hyper-spectral compact airborne spectral imager (CASI) imagery (one flight each year). Individual measurements are made on the ground at 2 m intervals for LiDAR and 1 m resolution for CASI. In this study, the LiDAR DSM of 2001 is used (Fig. 2). These images, geometrically corrected by the Environment Agency, are spatial composites of multiple flight strips. The area covered by these images is approximately 6 km^2.

3.3. Segmentation of landforms from a LiDAR DSM

In our initial coastal landform analysis of the Ainsdale Sands, we performed a hierarchical splitting segmentation based on the joint $LBP_{c,j}$, VAR_c distribution (Lucieer et al., 2003). We selected the following four landform classes: beach flat, dune, dune ridge, and woodland.

Fig. 3a shows the result of this supervised segmentation of a 512×512 pixel subset of the LiDAR DSM of the study area. Four reference areas of 40×40 pixels were selected for training. Values for P and R were 8 and 1, respectively. An accuracy assessment of the segmentation results provided an overall accuracy of 85.59% and a Kappa coefficient of 0.81. Object uncertainty values provided useful information on the locations and extent of transition zones (Fig. 3b).

3.4. Multi-scale texture measures from a LiDAR DSM

Our segmentation results (Lucieer et al., 2003) provided an initial coarse segmentation of the area into four general landform classes. One of the main shortcomings of this algorithm was the scale on which the texture model operated. We used one neighborhood set with $P = 8$ and $R = 1$ to calculate the texture measures. We have concluded, that to identify landform objects, one has to model the local pattern at different scales, i.e. for different values for P and R to describe local patterns at different radii. For example, the characteristic pattern of a dune ridge might be described by combining several circular neighborhood sets. To better describe landform objects, $LBP_c^{8,1}$, $LBP_c^{8,5}$, $LBP_c^{8,10}$ and $VAR_c^{8,1}$, $VAR_c^{8,5}$, $VAR_c^{8,10}$ values are calculated for every pixel, corresponding to three circular neighborhood sets with 8 neighbors at radii of 1, 5, and 10 pixels respectively. Then, $LBP_c^{P,R}$ values are summed to derive LBP_c^3. Similarly for VAR_c^3, the variance of the pixels in all three sets is computed. Total variance is then assigned to the centre pixel of a local

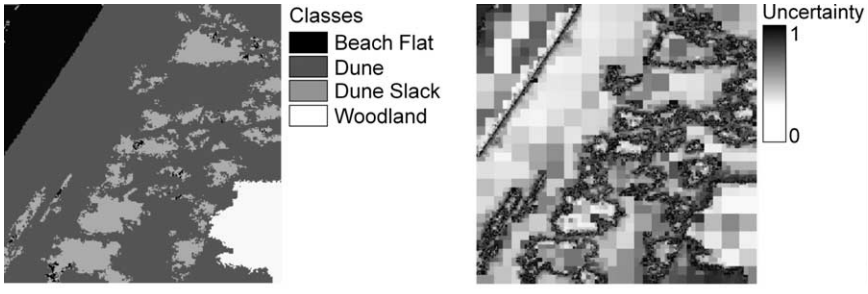

Fig. 3. Supervised texture-based segmentation: (a) segmentation result based on the joint $LBP_{c,j}$ and VAR_c distribution showing four landform classes; (b) related uncertainty for all object building blocks.

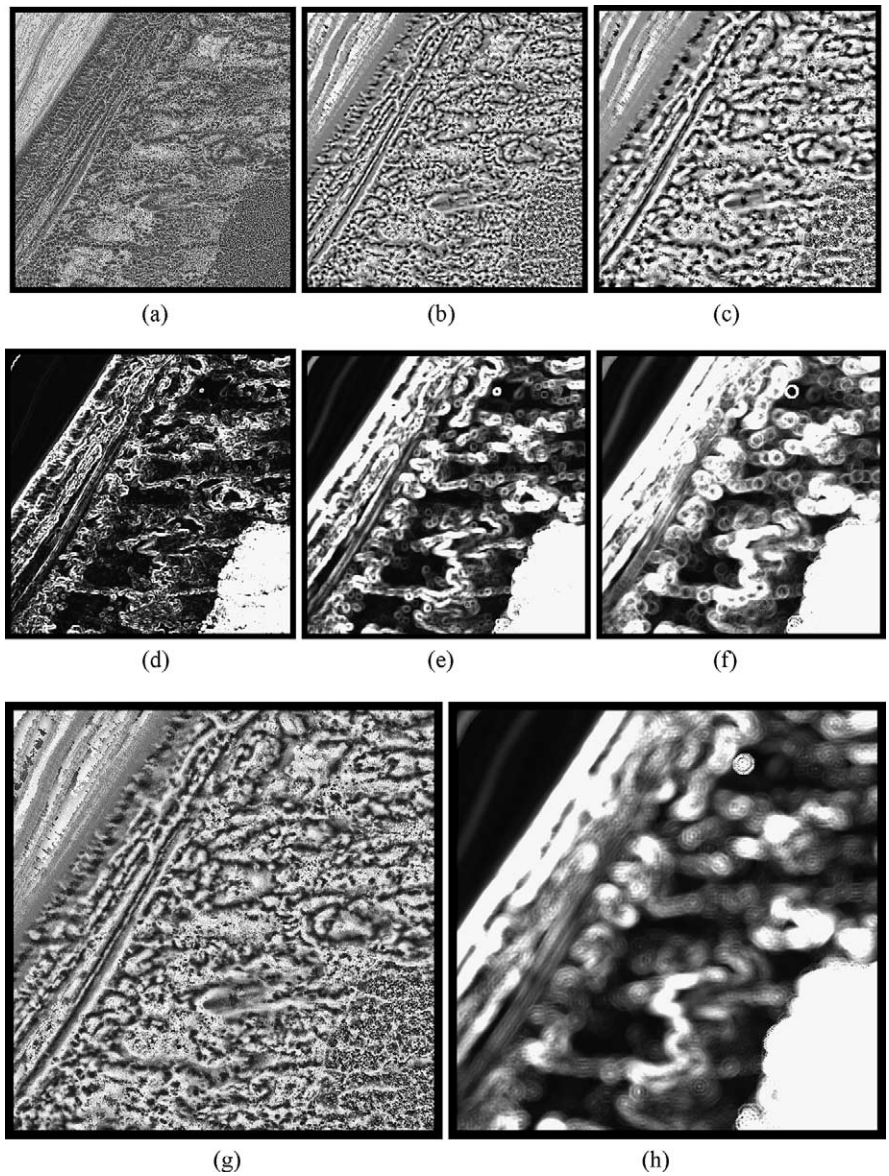

Fig. 4. Texture measures based in LiDAR DSM, shown in Fig. 2a: (a) image of $LBP_c^{8,1}$ values; (b) image of $LBP_c^{8,5}$ values; (c) image of $LBP_c^{8,10}$ values; (d) image of $VAR_c^{8,1}$ values; (e) image of $VAR_c^{8,5}$ values; (f) image of $VAR_c^{8,10}$ values; (g) summed LBP image with LBP_c^3 values; (h) image of total variance in three neighborhood sets VAR_c^3.

neighborhood. The result of these operations is given in Fig. 4. Landforms are more pronounced in these texture images. LBP_c^3 and VAR_c^3 images are combined with the DSM to form a three-band composite as input for the region growing algorithm (Fig. 5a).

3.5. Texture-based region growing

For identification of landform objects, we applied a texture-based seeded region growing algorithm. As a similarity criterion, we used the angle between the mean vector of an object and the feature vector of an

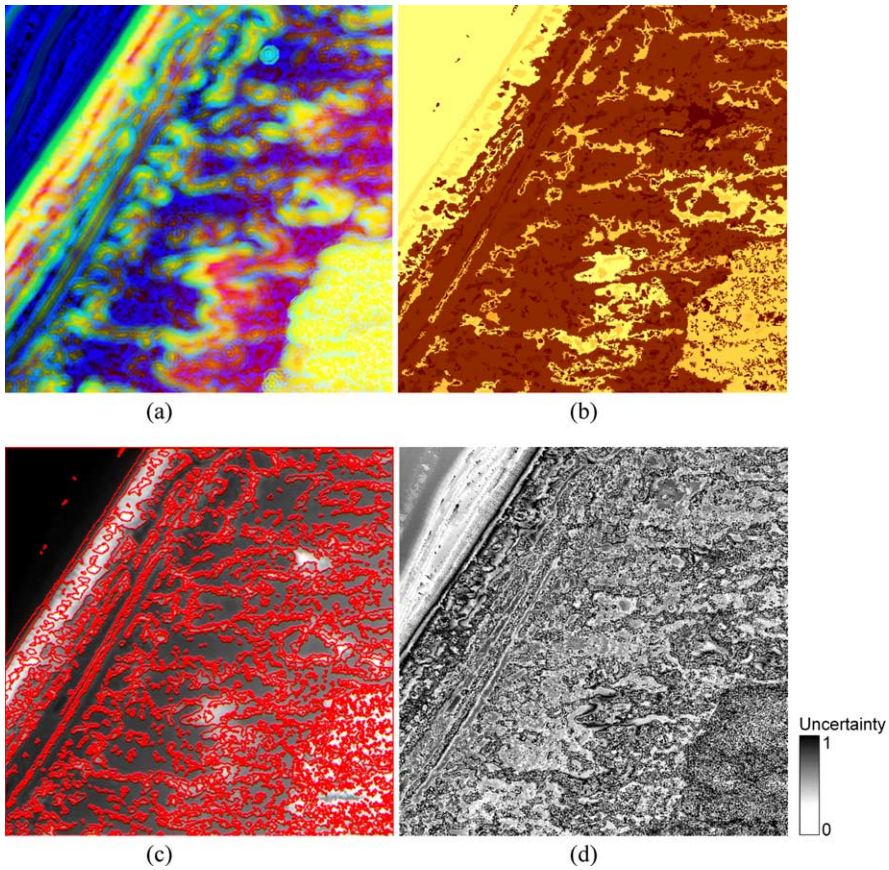

Fig. 5. Region growing results: (a) color composite of elevation, LBP_c^3 and VAR_c^3 values used as input for region growing segmentation; (b) objects as identified by the region growing algorithm. Color scheme is based on order of object ID-values; (c) object contours; (d) uncertainty values for each pixel, depicting uncertainty in object spatial extent.

adjacent pixel. The selected threshold was 0.30 radians. Initially 6006 objects were formed. After merging of neighboring objects in four iterations, 1446 objects remained. Fig. 5b shows the segmentation result. Segmentation was unsupervised, resulting in objects with numbered labels representing the order in which the objects were identified. Object boundaries were extracted and plotted on the original LiDAR DSM for object identification (Fig. 5c). Additionally, similarity measures for every pixel provided information on extensional uncertainty. If a pixel has a high similarity with an object, it has a small angle in feature space and therefore a low uncertainty value. Dark values in Fig. 5d depict pixels with high uncertainty.

Fig. 5b clearly shows landform objects. The beach flat was segmented as one homogeneous object. Its overall uncertainty value was low. Dune ridges were identified correctly, they corresponded to the ridges as observed in the field. The foredune was segmented as one homogeneous object. The dune ridges, located southeast of (and parallel to) the foredune are shown as long thin objects in the segmented image (Fig. 5b). In addition, several parabolic dune ridges can be observed. The lower parts of these dunes were segmented as separate objects. These lower objects corresponded to blowout areas, as observed in the field. The woodland area was different from the dune area, as its variance in texture was high. This was caused by the irregular LiDAR signal from the pine trees. The woodland area was identified as a collection of small objects, instead of a single homogeneous object. Uncertainty values were high for these small objects. In addition, uncertainty values were high in boundary areas of dunes and dune troughs (Fig. 5d).

High uncertainty values along the foredune show that there is a transition zone from the foredune object to the beach object.

4. Discussion and conclusions

In this study, we implemented and applied a region growing algorithm to derive landform objects from a LiDAR DSM based on image texture. Image texture was modeled with the local binary pattern (LBP) operator and local variance. We extended the standard $LBP_{c,j}$ and $VAR_{c,j}$ texture measures with a multi-scale neighborhood set. Compared to a local texture measure, a multi-scale approach provided a better landform description. The combination of the multi-scale LBP_c^N and VAR_c^N measures and the original elevation data, provided input for a region growing segmentation algorithm. Initial seed pixels were placed based on minimum local variance. These seeds were used to form initial objects. Merging of objects and adjacent pixels was based on a similarity criterion of the angle between the mean vector of the object and the feature vector of an adjacent pixel. After all image pixels were assigned to an object, neighboring objects were merged according to the same similarity criterion. Since the procedure was unsupervised, the identified objects were assigned numeric labels.

As an application, a LiDAR DSM of a coastal area in England was segmented into coastal landform objects. The texture-based region growing segmentation provided meaningful objects from the LiDAR DSM. Additionally, a pixel uncertainty value was based on a similarity measure, i.e. a large angle between an object mean vector and a neighboring pixel feature vector was interpreted as a high uncertainty value. These uncertainty values provided valuable information about transition zones between fuzzy objects.

In this study, an unsupervised approach was taken towards object identification. The advantage is that it provides an objective and automated technique for landform mapping. The identified objects, however, do not have class labels. Classification could be a subsequent step in landform analysis. Landform objects might be used in an object-based classification. Information on elevation distribution, texture distribution, object shape, topology, and semantics could be used to classify objects into meaningful landform classes.

Validation of landform objects is a difficult task. In this study, the most up to date and most accurate elevation data available were used. The dynamic nature of the coastal environment made validation complicated, as an accurate landform map of the same acquisition date was unavailable. Even if appropriate reference data would be available, validation itself is not straightforward. Object validation is most often based on boundaries. As shown in this study, coastal objects have a fuzzy nature, i.e. there are transition zones between objects. Therefore, boundary matching would be a difficult task as fuzzy objects only have an arbitrary boundary. Therefore, object validation was neither feasible nor meaningful in this study. From field observations, however, it could be concluded that good segmentation results were obtained. The described texture-based region growing algorithm is not restricted to coastal landform mapping. It can easily be applied to other remote sensing images and other study areas.

References

Ainsdale Sand Dunes NNR, 2003. English Nature National Natural Reserves. Last accessed: 24 January 2003. URL: http://www.english-nature.org.uk.

Cheng T., Fisher P.F., Rogers, P., 2002. Fuzziness in multi-scale fuzzy assignment of duneness. In: Proceedings of the International Symposium on Spatial Accuracy Assessment in Natural Resources and Environmental Sciences, Accuracy 2002, pp. 154–159.

Cheng, T., Molenaar, M., 2001. Formalizing fuzzy objects from uncertain classification results. Int. J. Geogr. Informat. Sci. 15, 27–42.

Fisher, P.F., Cheng, T., Wood, J., 2004. Where is Helvellyn? Multi-scale morphometry and the mountains of the English Lake District. Trans. Inst. Br. Geographers 29, 106–128.

Gorte, B.H.H., Stein, A., 1998. Bayesian classification and class area estimation of satellite images using stratification. IEEE Trans. Geosci. Remote Sens. 36, 803–812.

Haralick, R.M., Shanmugam, K., Dinstein, I., 1973. Textural features for image classification. IEEE Trans. Systems Man Cybernetics 2, 610–621.

Haralick, R.M., Shapiro, L.G., 1985. Image segmentation techniques. Comput. Vision Graphics Image Process. 29, 100–132.

Horowitz, S.L., Pavlidis, T., 1976. Picture segmentation by a tree traversal algorithm. J. Assoc. Comput. Machinery 23, 368–388.

Lucieer, A., Stein, A., 2002. Existential uncertainty of spatial objects segmented from remotely sensed imagery. IEEE Trans. Geosci. Remote Sens. 40, 2518–2521.

Lucieer, A., Stein, A., P.F. Fisher, 2003. Texture-based segmentation of high-resolution remotely sensed imagery for identification of fuzzy objects. In: Proceedings of the GeoComputation 2003. Southampton, UK (CDROM).

Nixon, M.S., Aguado, A.S., 2002. Feature Extraction and Image Processing. Butterworth-Heinemann.

Ojala, T., Pietikäinen, M., Mäenpää, T., 2002. Multiresolution gray-scale and rotation invariant texture classification with local binary patterns. IEEE Trans. Pattern Anal. Machine Intell. 24, 971–987.

Pietikäinen, M., Ojala, T., Xu, Z., 2000. Rotation-invariant texture classification using feature distributions. Pattern Recognit. 33, 43–52.

Randen, T., Husøy, J.H., 1999. Filtering for texture classification: a comparative study. IEEE Trans. Pattern Anal. Machine Intell. 21, 291–310.